RSC Advances

ROYAL SOCIETY OF CHEMISTRY

www.rsc.org/advances

RA-ART-08-2015-017214R1

New 13-pyridinealkyl berberine analogues intercalate to DNA and induce apoptosis in HepG2 and MCF-7 cells through ROS mediated P53 dependent pathway: biophysical, biochemical and molecular modeling studies†

Sabyasachi Chatterjee,[a] Sumana Mallick,[b] Franco Buzzetti,[c] Gaetano Fiorillo,[c] Tanjia Monir Syeda,[c] Paolo Lombardi,[c] Krishna Das Saha[b] and Gopinatha Suresh Kumar[a*]

[a]Biophysical Chemistry Laboratory, Organic and Medicinal Chemistry Division, CSIR-Indian institute of Chemical Biology, Kolkata 700 032, India

[b]Cancer Biology and Inflammatory Disorder Division, CSIR-Indian Institute of Chemical Biology, Kolkata 700 032, India

[c]Naxospharma srl, Via G. Di Vittorio, 70, 20026 Novate Milanese (MI), Italy

Address for Correspondence

Dr. G. Suresh Kumar, Ph.D

Senior Principal Scientist, Biophysical Chemistry Laboratory

CSIR-Indian Institute of Chemical Biology

4, Raja S.C. Mullick Road, Kolkata 700032, India

Phone: +91 33 2472 4049, Fax : +91 33 2472 3967

Email: gskumar@iicb.res.in

† Electronic supplementary information (ESI) available, see DOI:

RA-ART-08-2015-017214R1

Abstract

A new series of 13-pyridinealkyl berberine analogues were synthesized and their DNA binding efficacy studied by employing spectroscopic, calorimetric and molecular modeling techniques. Analogues with more than one CH_2 group showed better intercalative binding than berberine. The analog with one CH_2 group bound DNA weaker than berberine. The binding of the analog with single CH_2 group was entropy driven, while those with more than one CH_2 group was favored by both entropy and enthalpy changes. Higher salt concentration and temperature destabilized the binding. A larger contribution from non-polyelectrolytic forces to the Gibbs energy and the involvement of strong hydrophobic interactions were inferred. Molecular modeling pin pointed the specific binding site and the non-covalent interactions in the association.

The best DNA binding analogue inhibited the growth of hepatocellular and breast carcinoma most efficiently. It induced apoptosis in HepG2 and MCF-7 cells with externalization of phosphatidylserine and reactive oxygen species generation with accumulation of cells in the G0/G1 phase. Furthermore, up regulation of p53 and p21 indicated the role of p53 in BER5 mediated apoptosis. The results suggested that 13-pyridinealkyl berberine analogues intercalated to DNA much stronger than berberine, the chain length of the linker plays an important role for the binding, and they induced ROS mediated apoptosis in HepG2 and MCF-7 cells by p53 modulation.

RA-ART-08-2015-017214R1

Introduction

In cellular system, DNA is frequently targeted by low molecular weight ligands. DNA targeted therapeutic agents can interfere with numerous biological functions, the most important being the transcription and replication of DNA. Such interference can effectively retard or prevent cell division leading to chemotherapeutic action. A large spectrum of such DNA targeting drugs have been studied since the discovery of the DNA structure. Some like doxorubicin, dactinomycin, quarfloxin, mitoxantrone, mitomycin C, cisplatin were clinically employed, while many others are under different stages of investigation and clinical trial.

Berberine (Scheme 1a), a natural isoquinoline plant alkaloid of the structural class protoberberines, has many remarkable biological properties, the most potent albeit less investigated being its anticancer activity. A number of interesting studies, both in vitro and in vivo, on the antineoplastic activity of berberine have been reported in the literature that provide potential leads to promising futuristic clinical application for this alkaloid.[1-6] Nucleic acids are believed to be cellular targets of berberine in manifesting its anticancer activity and consequently many structural studies in this direction have been performed. An oligonucleotide-berberine complex has been recently crystallized and the structure solved.[7] The DNA binding studies have also been reviewed extensively in many recent articles.[8,9] Berberine has the unique distinction of exhibiting remarkable adenine-thymine base pair specificity unlike most other anticancer drugs that are specific to guanine-cytosine sequences.[10] But the critical limitations of berberine to be employed as a pharmaceutical preparation are *inter alia* its poor solubility, low

RA-ART-08-2015-017214R1

bioavailability and moderate nucleic acid binding affinity. To circumvent these problems attempts have been made to form inclusion complexes, nanoformulations, etc., that have met with only limited success.[11-13] It has thus become apparent that more effective derivatives with enhanced DNA and or RNA binding efficacy are essential for harnessing the anticancer activity of berberine. Recently a number of berberine (BER) analogues with aromatic moieties incorporated at the 13-position were reported to be more effective than berberine in exerting anticancer activity delaying the development of tumors.[5,14-15]

In this study, a series of novel 13-pyridinealkyl berberine analogues (Scheme 1b) were synthesized and their DNA binding activity investigated by various biophysical experiments and molecular modeling studies. These analogues are named BER1, BER2, BER3, BER4 and BER5 based on the number of methylene groups in the linker chain. We observed the most efficient binding with BER5 bearing the highest number of CH_2 groups in the series. Furthermore, these 13-pyridinealkyl berberine analogues induced apoptosis in HepG2 and MCF-7 human tumour cell lines. Reactive oxygen species (ROS) play pivotal roles in DNA damage [16] and p53 plays a role as downstream effecter of ROS.[17] The function of redox homeostasis in p53-regulated processes is a topic of great interest. Taken together, this work provides new fundamental knowledge and molecular mechanisms for the anticancer action of berberine analogues that may help further development as antineoplastic therapeutics.[5,6,18,19]

RA-ART-08-2015-017214R1

Results and discussion

Characterization of specific alkaloid-DNA association by spectroscopic analysis

These 13-pyridinealkyl berberine analogues possess an extra anchoring site. The binding of these analogues was initially probed by absorption spectroscopy titration methodology. The 13-pyridinealkyl analogues, like berberine, have characteristic absorption spectra in the region of 300−550 nm. The major peak maximum of the analogues varied around 340 nm and the spectral nature and features were similar. In this region DNA has negligible absorbance.

In the absorption spectral titration, hypochromic and bathochromic effects were observed with the occurrence of isosbestic points for all the analogues on titration with DNA. The representative absorbance titration profile of BER5 with Calf thymus (CT) DNA is depicted in Fig. 1A. The titration profiles of other analogues are presented in Fig. S1 (ESI†). The changes observed in the absorption spectra of BER5 are characteristic features of DNA intercalating ligands, revealing that the isoquinoline chromophore is stacked between the DNA base pairs in an intercalated posture. Equilibrium binding is confirmed from the presence of isosbestic points involving two state systems comprising of only free and bound alkaloid analogues. The alkaloid molecule along with the substituent moiety enters inside the DNA helix in such way that it is unable to form H-bonds with the solvent water molecules. The Scatchard plots of binding and subsequent McGhee-von Hippel analysis[20] of the absorption data (Fig. S2, ESI†) revealed that the BER shows cooperative binding manifested by negative slope at low r values.

RA-ART-08-2015-017214R1

These are described in details in the ESI†. On the other hand, the analogues present a non-cooperative binding mode with positive slope at low r values. So, the substitution of a pyridinealkyl group at the 13-position dramatically changes the nature of the binding from a non-cooperative mode to cooperative mode. This feature of these analogues is similar to that observed for 9 and 13-substituted analogues reported previously.[18,19,21] The equilibrium binding affinity values and the number of excluded sites i.e., the number of base pairs excluded by the binding of an alkaloid as per neighbor exclusion model, on the binding of these analogues are depicted in Table S1 (ESI†). The highest binding constant was observed for BER5 with five CH_2 groups in the linker and the affinity increased with increasing chain length except for BER1 where affinity was lower than BER. The number of excluded sites decreased with increasing chain length and was 6.6, 3.4, 3.2, 3.2 and 3.2, respectively, for BER1-5.

Berberine presents a weak intrinsic fluorescence property. The singlet excited state of the alkaloid returns to the ground state due to its intersystem crossing via nonradioactive mechanism.[22] The 13-pyridinealkyl berberine analogues exhibited more intense fluorescence than BER. The fluorescence intensity enhanced remarkably on binding with DNA. A representative spectral titration in the case of BER5 is presented in Fig. 1B and the titration profiles of analogues BER1-BER4 are presented in the Fig. S3 (ESI†). Change in the hydrophobic environment of the chromophore of the ligand due to transfer from a high polarity solvent environment to low polarity DNA interior when intercalated and consequent electronic interactions appear to cause this enhanced

RA-ART-08-2015-017214R1

fluorescence intensity. Furthermore, in the solution state rotational movement of the free alkaloid analogue molecules favor a radiation less deactivation of the excited states. But when bound to DNA in the intercalative mode the rotation is hindered and the deactivation through fluorescence emission is favoured, and a significant increase in the fluorescence intensity occurs.

Conformational changes in DNA measured by circular dichroism spectroscopy

The right handed helical conformation of B-form DNA showed a characteristic CD spectrum with a positive band in the 275−280 nm region and a negative band around 248 nm (Fig. 2A). The long wavelength band arises due to the base stacking interactions and the 248 nm band is due to the helicity.[23] The alkaloid analogues have no chiral center and hence are CD inactive. In an alkaloid-DNA titration study, the molar ellipticity value of the positive band increased with a small red shift of the wavelength maximum while the negative band changed only marginally. These features were similar in all the cases. The maximum change was observed in the case of BER5 as shown in the Fig. 2A. From the nature of the data it may be divulged that the alkaloid analogue molecules bind to DNA helix leading to conformational changes within in the B-form helical organization. It was also observed that a weak induced circular dichroism band appeared in the 340 nm region as shown in the Fig. 2B which is near the absorption maxima of the analogues. The result revealed that the alkaloid analogues bind in between the base pairs of the DNA helix by intercalation and due to this the helical chirality of DNA has changed. The induced CD spectrum arises from the strong

RA-ART-08-2015-017214R1

interaction of the electric transition moments of the analogues and the transition moments of the chirally arranged DNA bases/base pairs.

Thermal stabilization of the DNA helix by the alkaloids

Optical thermal melting experiments were carried out to understand the stabilization of the DNA helix on binding of the berberine analogues. The melting profile of DNA, monitored at the absorbance maximum (260 nm), revealed a cooperative hyperchromic transition of ~40% with a melting temperature (T_m) around 65 ^oC under the conditions employed here. Berberine stabilized DNA by about 7^oC. The binding of BER5 induced the highest stabilization and the melting temperature was around 85 ^oC (ΔT_m = 20^oC). With the exception of BER1 (ΔT_m = 5 ^oC) all the analogues stabilized DNA more than BER. The results are presented in Table S2 and the corresponding melting profiles are shown in Fig. S4 (ESI†).

The DNA stabilization was also confirmed by differential scanning calorimetry (DSC) experiments. The endothermic DNA peak was shifted to higher temperatures due to the binding of the alkaloid analogues. The ΔT_m values were 8.00, 4.19, 13.33, 16.75, 17.94 and 19.57 ^oC, respectively, for BER and BER1 to 5. These values are close to those obtained from optical melting experiments. The results are depicted in Table S2 (ESI†).

Elucidation of the mode of binding of the alkaloid analogues by fluorescence quenching and viscosity methods

BER is known to bind to DNA by an intercalative mode.[7,9,10] But to understand the mode of binding of the analogues we applied the fluorescence quenching technique and viscosity measurements. Fluorescence quenching using ferrocyanide ions, an anionic

RA-ART-08-2015-017214R1

quencher, has been effectively used to distinguish between intercalation and groove-binding modes of berberine analogues[18] and other small molecules [24-26]

The Stern−Volmer plots for fluorescence quenching of the BER and its analogues-DNA complexes by ferrocyanide ions are presented in Fig. S5 (ESI†). The results indicated that free analog molecules were quenched efficiently by the ferrocyanide ions. More fluorescence quenching was observed in the case of BER1 than BER and the effect gradually decreased for bound BER2−5, indicating that the bound analogues BER2−5 are located in a relatively more protected environment inside the DNA helix compared to those unbound. The Stern-Volmer quenching constants (K_{sv}) calculated were in the range 215−230 M^{-1} for the unbound BER and analogues, and 95, 170, 80, 71, 39 and 33 M^{-1}, respectively, for bound BER and BER1−5. The trend in the values revealed that the K_{sv} of BER1 was higher than that of BER and for the others it varied as BER>BER2> BER3> BER4>BER5. Based on this data it can be inferred that BER1 is a weaker intercalator than BER, while BER2-BER5 are better intercalators than BER. The pyridyl group of BER1 and the isoquinoline chromophore are separated by a single (CH_2) group and therefore the side chain linker appears to be too close to the isoquinoline chromophore leading to inhibition of the intercalation BER1. With gradual increase of the number of CH_2 groups in the linker chain, intercalation capability was found to increase and it became maximum for BER5. This was also clearly evident from the viscosity data, where the helix length enhancement due to intercalation was maximum with BER5. A plot of relative increase in length of rod like DNA (L/Lo) versus r, where r is the number of berberine analog molecules bound per mol of the nucleotide, is

RA-ART-08-2015-017214R1

presented in Fig. S6 (ESI†). The slope of the plots (β values) for BER and BER1-BER5 binding to DNA was found to be 0.66, 0.56, 0.70, 0.76, 0.83 and 0.90, respectively. Taken together, these results confirmed the intercalation of these analogues to DNA and also suggested a better intercalation geometry for BER2-5 compared to BER and provided evidence that the linker chain with more than one CH_2 group decisively contributes to the stronger intercalative binding of the isoquinoline moiety.

Thermodynamics of berberine analogues-DNA association

The thermodynamic profile of the interaction, that may provide key insights into the nature of the molecular forces that drive the complexation, was obtained from isothermal titration calorimetry (ITC) studies. Figure 3 A, B shows the representative ITC profiles of BER1 and BER5-DNA interaction. For BER5 the binding was exothermic in nature (Fig. 3A) but for BER1 (Fig. 3B) it showed endothermic heats. The ITC profiles in all the other cases were exothermic in nature. The presence of only one binding event in the thermogram in each case enabled the fitting of the isotherms to 'one set of binding sites' model yielding the best fit curve providing the equilibrium association constant (K), the stoichiometry (N) and the change in enthalpy ($\Delta_r H^o$). The entropy contribution ($T\Delta_r S^o$) and the standard change in molar Gibbs energy ($\Delta_r G^o$) were calculated as described previously.[18] The data obtained from the ITC experiments are summarized in the Table 1. A comparative chart depicting the variation of the K values of the analogues are shown in Fig. 3C. In all the cases except BER1 the binding was favoured by negative enthalpy and positive entropy changes. In the case of BER1, the

RA-ART-08-2015-017214R1

binding had an unfavorable enthalpy term. The small positive enthalpy for the binding was unfavourable to the Gibbs energy. The large entropy contribution in the binding of

Table 1. ITC derived thermodynamic parameters for the binding of berberine analogs with DNA[a]

Alkaloid analogue	Binding constant (K) x$10^5$$M^{-1}$	Stoichiometry (N)	(Δ_rG^0) kcal/mol	(Δ_rH^0) kcal/mol	($T\Delta_rS^0$) kcal/mol
BER	1.09 ± 0.07	0.482±0.03	-6.75±0.53	-2.834 ± 0.13	3.92
BER1	0.46 ± 0.08	0.161±0.08	-6.25± 0.98	0.89 ± 0.18	7.14
BER2	2.14 ±0.05	0.471 ±0.02	-7.07± 0.96	-1.80 ± 0.06	5.27
BER3	3.27 ± 0.33	0.361±0.07	-7.39± 0.90	-1.42 ± 0.09	5.97
BER4	6.45 ± 0.08	0.356±0.02	7.78± 0.61	-1.190 ± 0.06	6.59
BER5	9.96 ± 0.05	0.352±0.05	-8.04± 0.77	-1.04 ± 0.09	7.00

[a]The ITC experiments were conducted at a pressure of 101.10 kPa at 20 °C. K, the binding constant, N, the binding stoichiometry and Δ_rH^o, the standard molar enthalpy change were evaluated from ITC profiles fitting to Origin 7.0 software using the 'one set of binding sites' model. The values of Δ_rG^o, standard molar Gibbs energy change and $T\Delta_rS^o$, the standard molar entropy contribution were determined using the equations $\Delta_rG^o = \Delta_rH^o - T\Delta_rS^o = -RT\ln K$. R is the universal gas constant (1.98722 cal $K^{-1} \cdot mol^{-1}$.

RA-ART-08-2015-017214R1

BER1 compared to BER and other analogues can interpreted in terms of release of bound water and condensed sodium ions from the DNA grooves. This is because the pyridinealkyl moiety in BER1 appears to be very close to the isoquinoline chromophore of berberine leading to steric effects preventing BER1 from intercalating strongly between the DNA base pairs. This is also corroborated from the lower binding affinity of BER1 compared to all other analogues and even BER. A similar phenomenon was also reported previously for the DNA binding of 13-phenylalkyl berberine analogues.[18]

Ionic strength and temperature dependence of the binding

As the berberine analogues are cationic in nature it is expected that ionic interactions might play a leading role in the complexation process. It was observed that the ionic strength of the medium had significant influence on the binding of analogues in many previously reported studies.[18,27] To check on the nature of binding forces involved, the effect of ionic strength on the binding was investigated by ITC experiments in conjunction with van't Hoff analysis in the case of the strongest binding analogue, i.e., BER5 as a representative case. The thermodynamic parameters of the binding at three $[Na^+]$ concentrations investigated, viz. 10, 30 and 50 mM $[Na^+]$, were evaluated and the results are collated in Table S3 (ESI†). Increased $[Na^+]$ concentration results in reduced electrostatic repulsion between the negatively charged phosphate groups of adjacent nucleotides, and consequently the binding of BER5 to DNA was hindered, and the

RA-ART-08-2015-017214R1

equilibrium constant of the complexation decreased; at 30 mM, the binding affinity was 4.6×10^5 M^{-1} which was about half of that at 10 mM [Na^+].

A relation linking the equilibrium constant with the Na^+ ion concentration based on polyelectrolytic theories of Manning's counter ions condensation model[28] has been derived as follows

$$\left(\frac{\partial \log K}{\partial \log[\mathrm{Na}^+]}\right)_{T,P} = -z\psi$$

In this relation, Z is the apparent charge on the berberine analog and ψ is the fraction of sodium ions bound per phosphate group of the DNA. The number of ions released on the binding of a single BER5 molecule to DNA was calculated to be - 0.70 from the slope of the plot of log *K* versus log[Na^+]. From the dependence of *K* on [Na^+], the observed Gibbs energy was partitioned between the polyelectrolytic (Δ_rG_{pe}) and non-polyelectrolytic (Δ_rG_t) components using the relationship

$$\Delta rG^0_{pe} = Z\psi\, RT \ln([\mathrm{Na}^+])$$

where Zψ is the slope of the van't Hoff plot. The values of $\Delta_rG^o_{pe}$ and $\Delta_rG^o_t$ at the three salt conditions are depicted in Table S3. It can be observed that the magnitude of $\Delta_rG^o_{pe}$ was much lower than that of $\Delta_rG^o_t$ at all the salt conditions studied and the latter remained more or less constant. So it can be concluded that non-polyelectrolytic forces dominated the binding interaction here. Similar results were reported for phenylalkyl substituted berberine analogues also.[18]

RA-ART-08-2015-017214R1

Valuable insights into the type and magnitude of forces involved in the binding process was also obtained from the heat capacity ($\Delta_r Cp^o$) data derived from the temperature dependant variation of $\Delta_r H^o$. Titration calorimetry experiments were performed at three different temperatures, viz. 10, 20 and 30 ^oC, respectively, for the binding of the analogue BER5. The thermodynamic parameters derived from these experiments are presented in Table S4 (ESI†). A plot of $\Delta_r H^o$ versus T is presented in Fig. 3D. From the slope of the plot the value $\Delta_r Cp^o$ was determined to be - 25.97 cal/mol K for BER5-DNA complexation. For berberine a value of -110 cal/mol K was reported earlier.[29] A negative heat capacity term is proposed to arise due to the removal of large amount of nonpolar surface from aqueous exposure upon complex formation resulting in dominant hydrophobic effects in the interaction and has been displayed by a number of small molecule binding to DNA and RNA. Deriving strength from these results it may be proposed that there is a strong hydrophobic element in the interaction of these berberine analogues with DNA.

Base pair specificity of BER5 from ITC experiments

Berberine is one of the few DNA intercalating molecules known to exhibit remarkable AT base pair specificity.[9,10] To evaluate the binding specificity of the analogues we studied the binding of BER5, as a representative case, to poly(dA).poly(dT) and poly(dG).poly(dC). From ITC results the equilibrium constant for the binding to poly(dA).poly(dT) and poly(dG).poly(dC were evaluated to be 2.26 x 10^6 M^{-1} and 4.96 x 10^5 M^{-1}, respectively. It may be noted that the AT polynucleotide binding affinity was about 22 times higher than that to the GC polynucleotide. So it can be ascertained

RA-ART-08-2015-017214R1

unequivocally that the AT base pair specificity of binding of berberine is faithfully reproduced in these analogues also.

Elucidation of the binding site of BER5 by molecular docking

Molecular docking studies provide some insight into the interaction between the drug and DNA, and the results may be correlated with the experimental data. Here we chosen two oligo nucleotides of different GC content of PDB identifier 258D (A) and 1JH1 (B). The BER5 molecule has two parts, one isoquinoline part (same as berberine) and an additional spacer arm of alkylpyridine part. In both cases the docking studies showed that the isoquinoline part is intercalated between the two base pairs of DNA and the additional alkylpyridine part formed H-bonding interactions with the base of the DNA molecule as shown in the Fig. 4. The distance between the H-bonding of N-atom of pyridine (BER5) and the C_6-NH_2 group of the adenine (DNA) is 2 Å for A and 2.3 Å for N-atom of pyridine and the C_2-NH_2 group of the guanine. The calculated binding energy values from theoretical studies due to binding with the oligomer were -8.59 and -7.90 kcal/mol, respectively. The theoretical studies also supported our ITC data of base pair specificity of the BER5 molecule.

Apoptotic effect of BER5 in HepG2 and MCF-7 human tumour cells

To evaluate the efficacy of the BER and its analogues against cancer, the compounds were tested for their cytotoxic effect against hepatocellular carcinoma (HepG2) and mammary (MCF-7) human carcinoma cell lines using the MTT assay. After 24 h treatment, it was found that among the five compounds, BER5 showed a higher degree of concentration-dependent increase in growth inhibition in HepG2 and MCF-7 cell

RA-ART-08-2015-017214R1

lines, having GI_{50} values of 15.7 and 33.2 μM, respectively (Fig. 5A and 5B). However, it exhibited minimal effect on Human embryonic kidney 293 (HEK-293) cell lines even at a concentration of 40 μM (Fig. 5C). Treatment with BER5 induced phosphatidylserine (PS) externalization in HepG2 and MCF-7 cells after 24 h treatment which is a hallmark of apoptosis. After 24h treatment the percentage of apoptotic cells was 28.1% and 15.6% as compared to 5.3% and 2.0% in the vehicle treated cells in HepG2 and MCF-7 cell lines (Fig. 5D). Cell cycle arrest at various phases of cell division precedes apoptosis. Treatment of HepG2 and MCF-7 cells with BER5 (GI_{50} concentration) for 24 h showed a gradual increase in the number of cells in the G0/G1 phase. The percentages of G0/G1 population for the control and BER5 treated HepG2 cells were 57.3 % and 67.5 %, respectively, and for MCF-7 were 50.5 % and 75.7 %, respectively, indicating that BER5 induced cell cycle arrest at G0/G1 phase for these two cell lines (Fig. 5E). These results clearly suggested that BER5 induced apoptosis in HepG2 and MCF-7 cells.

Effect of BER5 induced ROS generation on apoptosis

Reactive oxygen species (ROS) generation plays an important role in apoptosis, so it is necessary to investigate the ability of BER analogue to generate ROS. Cells were exposed to GI_{50} concentration of BER5 for 24 h and analyzed for the presence of ROS by flow cytometry. Generation of reactive oxygen species is a key factor of apoptotic cell death. A number of studies established that berberine induced ROS generation and this has been reviewed.[2] To further elucidate whether BER5 induced intra cellular ROS generation in HepG2 and MCF-7 cells, ROS content was measured by flow cytometry

RA-ART-08-2015-017214R1

with H_2DCFDA. Treatment of BER5 at GI_{50} concentration with HepG2 and MCF-7 cells exhibited significantly enhanced intracellular ROS levels (Fig. 6A).

Flowcytometric analysis revealed that the DCF fluorescence intensity in BER5 (GI_{50}) treated cells was much higher for HepG2 and MCF-7 cells with respect to the control, indicating a sharp increase in mean fluorescence intensity from the control to BER5 treated cells. Upon treatment with GI_{50} concentration of BER5, there was an increase in intracellular ROS generation as compared with the control set after 24 h, which was dampened upon pre-incubating with NAC. Following pre-incubation with NAC, DCF fluorescence intensity of the control was lower with respect to BER5 treatment which was higher for HepG2 and MCF-7 cells, (Fig. 6B). Moreover, pre-incubation with NAC also inhibited the growth inhibitory role of BER5 (Fig. 6C). From this study it may be inferred that BER5 induced death in HepG2 and MCF-7 cells precede via the ROS mediated pathway.

Apoptotic cell death triggered by BER5 results in ROS dependent P53 activation

HepG2 and MCF-7 cells lines have wild type p53, which generally has a role in apoptosis. Therefore, the role p53 activation in BER5 induced apoptosis was examined.

Treatment of HepG2 and MCF-7 cells with BER5 (GI_{50}) resulted in increased expression and translocation of p53 to the nucleus along with increased expression of p21 as compared to the control (Fig. 7A). The corresponding fluorescence intensity graphs are presented in Fig. S7 (ESI†). Moreover, cells that were incubated with 20 μM of pifithrin-a (an inhibitor of p53 transactivation) for 2 h prior to treatment with BER5 showed

RA-ART-08-2015-017214R1

inhibition in cytotoxicity by BER5, indicating that p53 may be involved in BER5 mediated apoptosis (Fig. 7C).

In order to evaluate whether ROS is involved in p53 activation or vice versa, HepG2 and MCF-7 cells were pre-incubated with NAC prior to BER5 treatment, which led to the suppression of p53 and p21 expression (Fig. 7B) whereas, incubation with pifithrin-a, prior to BER5 exposure failed to inhibit ROS production (Fig. 7D), indicating that ROS is acting upstream of p53 but not vice versa. Thereby, it can be concluded that p53 induced apoptosis in these cell lines is ROS dependent.

Compound intake by BER5

From the biophysical studies presented above it was established that among the five alkaloid analogues BER5 showed the highest affinity to DNA. Therefore, it has become important to understand the cellular uptake and sub-cellular distribution of BER5 in order to gain further mechanistic insights. Previous reports established that BER has fluorescence property.[30] BER5 exhibited fluorescence emission property and its fluorescence intensity was higher than BER and other analogues. From emission spectroscopy it was observed that upon binding to DNA the fluorescence intensity of BER5 increased (Fig. 1B). In order to visualize BER5 directly in the HepG2 and MCF-7 cells, cells were grown onto a cover slip and treated with BER5 as described in the experimental section, and was evaluated using a Confocal microscope at 12 h and 24 h time periods. DAPI was used as the nuclear marker. The fluorescence intensity of the analogue in cells was evaluated at 12 h and 24 h and it was found that at 12 h dense fluorescence intensity around nucleus (Fig. 8A) and at 24 h fluorescence was detected

RA-ART-08-2015-017214R1

inside the nucleus (Fig. 8B) which proved that with time BER5 enters the cell nucleus. The uptake of BER5 was measured by treating cells for 24 h with BER5 (GI_{50}) and measuring using flow cytometry which indicated a higher fluorescence in both HepG2 and MCF-7 cells as compared to the control (Fig. 8C).

Conclusions

Here we have presented results on the DNA interaction of five new berberine analogues with pyridinealkyl substitution at the 13-position of the isoquinoline chromophore. The results obtained from absorption and fluorescence studies suggested at first that the analogues bound to DNA stronger than berberine, and that the increased affinity is applicable only when the linker chain length was beyond one CH_2 group. Thus, a critical length was required for effecting higher binding. The binding affinity of the analogue BER5 was almost ten times higher than that of berberine. Unlike berberine, the analogues bound DNA in a cooperative manner and stabilized the DNA helix strongly against thermal strand separation. Similar results have been reported previously for analogues with substituents at 9- and 13-positions.[18,21] The binding of these analogues have been inferred to occur through intercalation based on the results from viscosity and fluorescence quenching experiments, and further confirmed from molecular modeling studies. The conformational changes effected in DNA on binding and the induced circular dichroism acquired by the analogues further substantiated their stronger binding over berberine. From calorimetry results it was revealed that the analogues bound to DNA by an entropy driven manner that is justified because of their long side chain that can effect strong disruption of the water structure in the grooves of

RA-ART-08-2015-017214R1

the DNA. Furthermore, the results of salt and temperature dependent studies proposed that the binding mostly involved non-polyelectrolytic forces which were corroborated from the value of the heat capacity change. Overall, the structural studies present a remarkably stronger affinity and better interaction profile of these analogues over berberine to DNA.

Among the five 13-pyridinealkyl berberine analogues, BER5 showed maximum cytotoxicity towards HepG2 and MCF-7 human tumour cells after 24 h, but in different degrees. Interestingly, 40 μM of BER5 did not show any toxic effects on normal HEK293 cells suggesting a potential therapeutic window. Significant annexin V-FITC positivity and accumulation of cells at G0/G1 phase had indicated that BER5 induced apoptosis in HepG2 and MCF-7 cells.

As HepG2 and MCF-7 cells are p53 wild type the role of p53 is quite relevant here. Pre-incubation with NAC resulted in an increase in cell viability in the presence of BER5 while pre-incubation with PFT-α did not prevent ROS generation. However, p21 the transcriptional targets of p53 was affected by the inhibitory role of NAC on ROS. BER5, therefore, may be inducing ROS generation upstream of p53 leading to apoptosis in the ROS mediated pathway. To conclude, BER5 mediates apoptosis in HepG2 and MCF-7 cells via a ROS mediated p53 dependent pathway and makes it a promising anticancer agent towards p53 wild type tumors.

Materials and methods

Materials

RA-ART-08-2015-017214R1

DNA from Calf thymus (CT, type XI, 42% guanine-cytosine composition), poly(dA)·poly(dT), poly(dG)·poly(dC), berberine chloride (BER), L-glutamine, 3-(4,5-dimethylthiazol-2-yl)-2,5-diphenyltetrazolium bromide (MTT), fetal bovine serum (FBS), streptomycin, penicillin, Dulbecco's modified eagle medium (DMEM), 4-2-hydroxyethyl-1-piperazineethanesulfonic acid (HEPES), JC-1, 6-diamidino-2-phenylindole dihydrochloride (DAPI), PI, Annexin V-FITC, and other general reagents were purchased from Sigma (St. Louis, USA). Antibodies against p53 and p21 were purchased from Cell Signalling (Danvers, USA). The biophysical experiments were performed in citrate-phosphate (CP) buffer of pH 7.4, containing 10 mM Na_2HPO_4. Concentration was measured in a spectrophotometer by using molar absorption coefficients (ε, in M^{-1} cm^{-1}) as follows. Calf thymus DNA : $13.2x10^2$ (at 260 nm),[18] poly(dA).poly(dT) : 13.6 $x10^2$ at 260 nm, poly(dG).poly(dC) : 16.8 $x10^2$ at 255 nm, berberine : 22.5 $x10^2$ (at 345 nm)[19] and all the 13-analogues: 21.3 $x10^2$ at their respective λ_{max}.

Synthesis of 13-pyridinealkyl berberine derivatives BER1-BER5

The 13-pyridinelalkyl berberine derivatives were claimed in US Pat. 8,188,109B2 to Naxospharma srl. These were synthesized starting from commercial sample of berberine chloride hydrate (ca. 17% H_2O, Shanghai Trust & We, China) and the appropriate pyridine (alkyl) carboxaldehydes (Fig. 1a), via a modification of a unusual enamine-aldehyde condensation performed on dihydroberberine[31] and purified by following the method of Weber.[32] The aldehydes were prepared starting from commercial pyridine-4-carboxaldehyde (Scheme 1b) or 4-(2-hydroxyethyl)pyridine

RA-ART-08-2015-017214R1

(Scheme 1c) (both purchased from Alfa Aesar GmbH & Co KG, Karlsruhe, Germany), following usual homologation and oxidation methods and procedures known in organic chemistry.

The purity (>94%) of the derivatives was ascertained on the Jasco HPLC LC-2000 series system (Jasco International, Europe) with an Agilent Eclipse XDB-C18 (4.6 mm x 150 mm x 3.5 mm) column (Agilent Technologies, USA) by applying a method by Weber. The rate of flow of the mobile phase (68% 30 mM ammonium acetate, 14 mM TEA, pH ~ 4.85, 32% acetonitrile) was maintained at 1 mL/min. and absorbance was measured at four wavelengths viz. 235, 265, 340, and 420 nm, respectively.

The structures of the derivatives were confirmed by ^{1}H NMR spectra measured on a Varian Mercury 400 MHz spectrometer.

13-[(pyridin-4-yl)methyl]-9,10-dimethoxy-5,6-dihydrobenzo[g]-1,3-benzodioxolo[5,6-a]quinolizinium chloride, BER1: (DMSO-d6), δ: 10.07 (s, 1H), 8.45 (ddd, 5H), 8.10 (d, 1H), 7.76 (d, 1H), 7.20 (d, 2H), 6.85 (s, 1H), 6.09 (s, 2H), 5.70 (s, 1H), 4.81-4.61 (t + s, 6H), 4.08 (d, 6H), 3.12 (d, 2H).

13-[2-(pyridin-4-yl)ethyl]-9,10-dimethoxy-5,6-dihydrobenzo[g]-1,3-benzodioxolo[5,6-a]quinolizinium chloride, BER2: (DMSO-d6), δ: 10.06 (s, 1H), 8.51 (d, 2H), 8.33 (d,2H), 8.08 (d, 1H), 7.73 (d, 1H), 7.18 (d, 1H), 7.05 (s, 1H), 6.83 (s, 1H), 6.08 (s, 2H), 4.09 (s, 6H), 3.14 (m, 2H), 2,82 (m, 2H).

13-[3-(pyridin-4-yl)propyl]-9,10-dimethoxy-5,6-dihydrobenzo[g]-1,3-benzodioxolo[5,6-a]quinolizinium chloride, BER3: ($CDCl_3$), δ: 10.35 (s, 1H), 8.52 (d, 1H), 8.05 (d, 1H), 7.88

RA-ART-08-2015-017214R1

(d, 1H), 7.64 (d, 1H), 6.88 (d, 2H), 6.15 (s, 1H), 5.09 (br, 2H), 4.33 (s, 3H), 4.06 (s, 3H), 3.44 (br, 2H), , 3.23 (br, 2H), 2.98 (br, 2H), 2.19 (br, 2H).

13-[4-(pyridin-4-yl)butyl]-9,10-dimethoxy-5,6-dihydrobenzo[g]-1,3-benzodioxolo[5,6-a]quinolizinium chloride, BER4: ($CDCl_3$), δ: 10.49 (s, 1H), 8.57 (d, 2H), 7.83 (s, 2H), 7.37 (d, 2H), 6.98 (s, 1H), 6.89 (s, 1H), 6.12 (s, 1H), 5.17 (br, 2H), 4.31 (s, 3H), 4.07 (s, 3H), 3.34 (t, 2H), 3.18 (t, 2H), 2.80 (br, 4H).

13-[5-(pyridin-4-yl)pentyl]-9,10-dimethoxy-5,6-dihydrobenzo[g]-1,3-benzodioxolo[5,6-a]quinolizinium chloride, BER5: (DMSO-d6), δ: 9.90 (s, 1H), 8.40 (d, 2H), 8.20 (d, 2H), 7.24 (d, 2H), 7.14 (s, 2H), 6.14 (s, 2H), 4.77 (br, 2H), 4.05 (s, 6H), 3.04 (br, 2H), 2.50 (m, 2H), 1.70 - 1.20 (m, 6H).

Methods

Spectroscopic studies

The UV-vis absorption studies used a Jasco V660 unit (Jasco International Co. Ltd., Hachioji, Japan). The methodology reported by Chaires[33] and described in details earlier was followed.[30,34,35] All the fluorescence experiments were carried out in a Quanta Master 400 unit (Horiba PTI, Canada) controlled with FelixGX spectroscopy software provided with the instrument. The temperature was controlled by EHEIM type-2232 307 (GmbH & COKG, Germany). The alkaloid analogues were excited at their absorption maxima near 345 nm.

CD spectropolarimetric studies

RA-ART-08-2015-017214R1

Circular dichroism spectropolarimetric experiments used a J-815 Jasco unit (Jasco International Co. Ltd.) equipped with a peltier cuvette holder and associated temperature programmer as reported earlier.[36-38]

Optical thermal melting experiments

A Pharmaspec 1700 unit (Shimadzu Corporation) with a peltier devise (TMSPC-8) was used for DNA melting experiments as described earlier.[18] A Teflon stoppered eight segment quartz cuvette (1 cm optical path length and 110 µl volume) was used for the melting experiments. DNA sample (20 µM) was mixed with varying concentrations of the alkaloid analog under study (upto D/P=1) and the mixture was heated at a rate of 0.5 °C/min, continuously monitoring the absorbance change at 260 nm. The melting temperature (T_m) is the midpoint of the transition profile as determined by the maxima of the first derivative plots.

Fluorescence quenching studies

Quenching experiments were performed with the negatively charged quencher $K_4[Fe(CN)_6]$ as described previously[18] and discussed in details in the electronic supplementary information. The data were analyzed by Stern-Volmer equation and plotted as relative fluorescence intensity versus the ferrocyanide ion concentration.

Hydrodynamic studies

The viscosity was determined by measuring the time of flow through a size 75 capillary viscometer from Cannon Instruments Company that was submerged in a thermostated water bath (20 ± 1 °C).[37] Relative viscosity of DNA in the absence and in the presence of

RA-ART-08-2015-017214R1

the alkaloid analogues was calculated by equations described in the electronic supplementary information.

Isothermal titration calorimetry

ITC experiments were performed using MicroCal VP-ITC unit (MicroCal, LLC, USA) as reported earlier.[30,38,39] The calorimeter was calibrated from time to time as per the manufacturer's protocols. Degassed alkaloid solutions (500 μM) were injected from the rotating syringe into the sample chamber that housed the DNA solution. For control experiments same protocol of injecting alkaloid into the experimental buffer was used. The heat generated in the dilution experiment was subtracted to give the heat profile for the DNA-alkaloid binding. The data were plotted as a function of molar ratio and fitted to the 'one site binding model' using Origin 7.0 software to provide the thermodynamic parameters ($\Delta_r H°$, N and K).

The following equations were used to evaluate $\Delta_r G°$.

$$\Delta_r G° = -RT \ln K$$

The binding entropy contribution ($T\Delta_r S°$) was evaluated by the relationship

$$T\Delta_r S° = \Delta_r H° - \Delta_r G°$$

In these equations R and T represent the universal gas constant and absolute temperature in Kelvin, respectively.

Differential scanning calorimetry

DSC experiments used a Microcal VP-differential scanning calorimeter (MicroCal, LLC). Detailed experimental procedures have been described previously.[30,40]

Docking studies

RA-ART-08-2015-017214R1

Short oligomeric DNA crystal structure of different GC- content for docking analysis, was extracted from Protein Data Bank (PDB) identifier 258D (GC content 33.33%) and 1JHI (GC content 66.66%). The BER5 molecule was drawn and the energy minimized by Avogadro 1.1.1 molecular editor. Docking studies were performed with the AutoDock 1.5.6 program, which utilizes the Lamarckian Genetic Algorithm (LGA). The water molecules were removed from the DNA molecule used for docking. Polar hydrogen and Gasteiger charges were added to prepare the DNA molecule for docking. Rotatable bond in the ligand was assigned with AutoDock tools in AutoDock. The DNA and DER5 were enclosed in the grid box that was set to 120, 120, and 120 Å along the X-, Y-, and Z-axis with a 0.414 Å grid spacing in order to recognize the binding site of BER5 in oligomer of 258D crystal structure and for 1JHI the grid box is 70, 60, 70 Å along the X, Y-, and Z-axis with a 0.375 Å. Other miscellaneous parameters were assigned as per the default values given by the AutoDock program. The lowest binding energy was chosen from among the most possible 10 docking conformations. The output from AutoDock was analyzed by PyMol.

Cell culture

HepG2 (human hepatocellular carcinoma), MCF-7 (human breast adenocarcinoma) and HEK-293 (human embryonic kidney 293) cell lines were obtained from National Centre for Cell Science, Pune, India. All cells were grown in DMEM supplemented with 10% heat inactivated fetal bovine serum (FBS) and 1% antibiotic-antimycotic, in a humidified atmosphere at 37^{o}C with 5% CO_2.

Cell viability assay

RA-ART-08-2015-017214R1

Cancer cells were treated in the presence of different concentrations of BER, BER1, BER2, BER3, BER4 and BER5 (0, 10, 20, 30, and 40 µM) dissolved in CP buffer and their respective GI_{50}'s were determined in HepG2 and MCF-7 cell lines by MTT assay as described earlier.[40] In another set of experiment, HEK-293 cells were treated with BER5 (0-40 µM) for 24 h. Absorbance of the formazan was measured at 595 nm using an ELISA reader.

Detection of apoptosis by flow cytometry

Measurement of apoptosis was performed by using an annexin V-FITC apoptosis detection kit as described.[40] MCF-7 and HepG2 cells were treated with BER5 (GI_{50}) for 24 h and stained according to the protocol of the manufacturer. The % of live, apoptotic and necrotic cells were analyzed in cell BD LSR Fortessa cell analyzer (Becton Dickinson, San Jose, CA, USA). 1 x 10^4 cells in each sample were analyzed.

Analysis of cell cycle arrest

Cells were treated with BER5 for 24 hours. This was followed by PI staining and cell cycle arrest analysis, as described.[40] The percentage of cell population undergoing cell cycle arrest were analyzed. 1x10^4 cells were analyzed for each sample.

Intracellular ROS measurements

Cells (1x10^6) were treated with BER5 for 24 h and the levels of intracellular H_2O_2 were assessed by flow cytometry after incubating with H_2DCFDA (20 mM) for 30 min at 37^{o}C. For inhibition of ROS generation, cells were pretreated with Nacetyl cysteine (10 mM) for 30 min before BER5 treatment. 1x10^4 cells were analyzed.[41]

Confocal microscopy for immunocytochemistry studies

RA-ART-08-2015-017214R1

HepG2 and MCF-7 cells were treated with BER5 (0 and GI_{50}) for 24 h and confocal microscopy for immunocytochemistry analysis of p53 and p21 was done as reported earlier.[41] In another set of experiments, cells were incubated with 2.5 mM of NAC 2 h prior to BER5 treatment and immunocytochemistry analysis of p53 and p21 was done. Cells were observed under an Andor spinning disk confocal microscope and images were acquired and fluorescence intensity measured using Image J 1.46 software.

Compound uptake and intracellular localization studies of BER5 using flow cytometry and confocal microscopy

To analyze quantitatively HepG2 and MCF-7 cells were seeded (1×10^5 for each sample) and BER5 was added. After 24 h of incubation cells were twice washed with PBS and analyzed using flow cytometry. To determine qualitatively, whether BER5 binds with DNA *in vitro*, HepG2 and MCF-7 cells were grown on cover slips with complete medium for 24 h and were incubated with GI_{50} concentration of BER5 for 12 h and 24 h at 37°C. At the end of incubation period, cells were washed with cold PBS and fixed with 3% paraformaldehyde for 15 min. at 4°C. DAPI (1 µg/ml) was added at room temperature for nuclear demarcation. After washing the cells twice with PBS and they were analyzed by confocal microscopy. Fluorescence was analyzed under an Andor spinning disk confocal microscope. Images were acquired and fluorescence intensity was measured using Image J 1.46 software.

Acknowledgments

This work was funded by grants from the Council of Scientific and Industrial Research (CSIR), Govt. of India net work project BSC0123 (GenCODE). S. Chatterjee is a Senior

RA-ART-08-2015-017214R1

Research Fellow supported by the University Grants Commission, Government of India. Authors express sincere thanks to Dr. S. N. Bhattacharyya, Principal Scientist and Mr. D. Sarkar of this institute for help during confocal microscopic analysis. Ms. A. Ganguly's assistance in flow cytometric study experiments is appreciated. Naxospharma srl, Italy, acknowledges financial support by the Italian Ministry of Economic Development (Grant No. 01705) under the 6th call of the EuroTransBio initiative, transnational project BER.T.A (BERberine as antiTumour Agents).

RA-ART-08-2015-017214R1

References

1 C. M. Tsang, Y. C. Cheung, V. W. Y. Lui, Y. L. Yip, G. Zhang, V. W. Lin, K. C. P. Cheung, Y. Feng and S. W. Tsao, *BMC Cancer*, 2013, **13**, 619.

2 Y. Sun, K. Xun, Y. Wang and X. Chen, *Anti Cancer Drugs*, 2009, **20**, 757-769.

3 S. Jantová, L.Cipák, M.Cernáková and D. Kost'álová, *J. Pharm. Pharmacol.*, 2003, **55**, 1143–1149.

4 J.P. Lin, J.S. Yang, J.H. Lee, W.T. Hsieh and J. G. Chung, *World J. Gastroenterol.*, 2006, **12**, 21-28.

5 L. M. Guamàn Ortiz, P. Lombardi, M. Tillhon and A. I. Scovassi, *Molecules*, 2014, **19**, 12349-12367.

6 L. M. Guamàn Ortiz, M. Tillhon, M. Parks, E. Prosperi, M. Savio, A. G. Arcamone, F. Buzzetti, P. Lombardi and A. I. Scovassi, *Biomed. Res. Int.*, 2014, ID 924585.

7 M. Ferraroni, C. Bazzicalupi, A. R. Biliab and P. Gratteri, *Chem. Commun.*, 2011, **47**, 4917–4919.

8 M. Maiti and G. Suresh Kumar, *J. Nucleic Acids*, 2010 Article ID 593408, 23 pages.

9 K. Bhadra and G. Suresh Kumar, *Med. Res. Rev.,* 2011, **31**, 821-862.

10 D. Debnath, G. Suresh Kumar, R. Nandi and M. Maiti, *Indian J. Biochem. Biophys.*, 1989, **26**, 201-208.

11 M. Halimani, S. P. Chandran, S. Kashyap, V. M. Jadhav, B.L.V. Prasad, S. Hotha and S. Maiti, *Langmuir*, 2009, **25**, 2339-2347.

12 S. Hazra, M. Hossain and G. Suresh Kumar, *J. Incl. Phen. Macrocycl. Chem.* 2014, **78**, 311-323.

13 S. P. Liu, Z. Yang, Z.F. Liu, J. T. Liu and Y. Shi, *Anal. Chim. Acta.*, 2006, **572**, 283–289.

14 E. Pierpaoli, V. Viola, A. Barucca, F. Orlando, F. Galli and M. Provinciali, *Carcinogenesis*, 2013, **34**, 1352-1360.

15 E. Pierpaoli, E. Damiani, F. Orlando, G. Lucarini, B. Bartozzi, P. Lombardi, C. Salvatore, C. Geroni, A. Donati and M. Provinciali, *Carcinogenesis*, 2015, doi: 10.1093/carcin/bgv103).

16 D. Trachootham, J. Alexandre and P. Huang, *Nature Rev. Drug Discovery*, 2009, **8**, 579-591.

17 B. Liu, Y. Chen and D. K. St Clair, *Free Radicals Biol. Med.*, 2008, **44**, 1529–1535.

18 D. Bhowmik, M. Hossain, F. Buzzetti, R. D'Auria, P. Lombardi and G. Suresh Kumar, *J. Phys. Chem. B*, 2012, **116**, 2314−2324.

19 D. Bhowmik, F. Buzzetti, G. Fiorillo, F. Orzi, T. M. Syeda, P. Lombardi and G. Suresh Kumar, *MedChemComm.*, 2014, **5**, 226-231.

20 J. D. McGhee and P. H. von Hippel, *J. Mol. Biol.* **1974**, *86*, 469-489.

21 A. Basu, P. Jaisankar and G. Suresh Kumar, *Bioorg. Med. Chem.*, 2012, **20**, 2498-2505.

22 K. Hirakawa, S. Kawanishi and T. Hirano, *Chem. Res. Toxicol.*, 2005, **18**, 1545-1552.

23 G. M. Hashem, J. D. Wen, Q. Do and D. M. Gray, *Nucleic Acids Res.*, 1999, **27**, 3371-3379.

24 M. M. Islam, P. Pandya, S. Roy Chowdhury, S. Kumar and G. Suresh Kumar, *J. Mol. Struct.*, 2008, **891**, 498-507.

25 S. Roy Chowdhury, M. M. Islam and G. Suresh Kumar, *Mol. Biosyst.*, 2010, **6**, 1265-1276.

26 A. Das and G. Suresh Kumar, *Biochim. Biophys. Acta*, 2013, **1830**, 4708-4718.

27 27.D. Bhowmik, F. Buzzetti, G. Fiorillo, L. Franchini, T. M. Syeda, P. Lombardi and G. Suresh Kumar, *J. Therm. Anal. Calorim.*, 2014, **118**, 461-473.

28 M. T. Record Jr., C. F. Anderson and T. M. Lohman, *Q. Rev. Biophys.*, 1978, **11**, 103-178.

29 K. Bhadra, M. Maiti and G. Suresh Kumar, *Biochim. Biophys. Acta*, 2008, **1780**, 1054–1061.

30 M. M. Islam, S. Roy Chowdhury and G. Suresh Kumar, *J. Phys. Chem. B,* 2009, **113**, 1210-1224.

31 K. Iwasa, M. Kamigauchi, M. Sugiura and H. Namba, *Planta Med.*, 1997, **63**, 196-198.

32 H. A. Weber, M. K. Zart, A. E. Hodges, H. M. Molloy, B. M. O'Brien, L. A. Moody, A. P. Clark and R. K. Harris, *J. Agric. Food Chem.*, 2003, **51,** 7352-7358.

33 J. B. Chaires, *Biochemistry*, 1983, **22**, 4204–4211.

34 K. Bhadra, M. Maiti and G. Suresh Kumar, *Biochim. Biophys. Acta*, 2007, **1770**, 1071-1080.

35 M. M. Islam, P. Pandya, S. Kumar and G. Suresh Kumar, *Mol. BioSyst.*, 2009, **5**, 244-254.

36 K. Bhadra, M. Maiti and G. Suresh Kumar, *Chem. Biodiversity,* 2009, **6**, 1323–1342.

RA-ART-08-2015-017214R1

37 M. M. Islam, R. Sinha and G. Suresh Kumar, *Biophys. Chem.*, 2007, **125**, 508−520.

38 R. Sinha, M. M. Islam, K. Bhadra, G. Suresh Kumar and M. Maiti, *Biorg. Med. Chem.*, 2006, **14**, 800-814.

39 M. Hossain and G. Suresh Kumar, *J. Chem. Thermodyn.*, 2010, **42**, 1273-1280.

40 S. Mallick, P. Ghosh, S. K. Samanta, S. Kinra, B. C. Pal, A. Gomes and J. R. Vedasiromoni, *Cancer Chemother. Pharmacol.*, 2010, **66**, 709-719.

41 A. Nandy, S. K. Dey, S. Das, R. N. Munda, J. Dinda and K. Das Saha, *Mol. Cancer*, 2014, 13**:** 57.

RA-ART-08-2015-017214R1

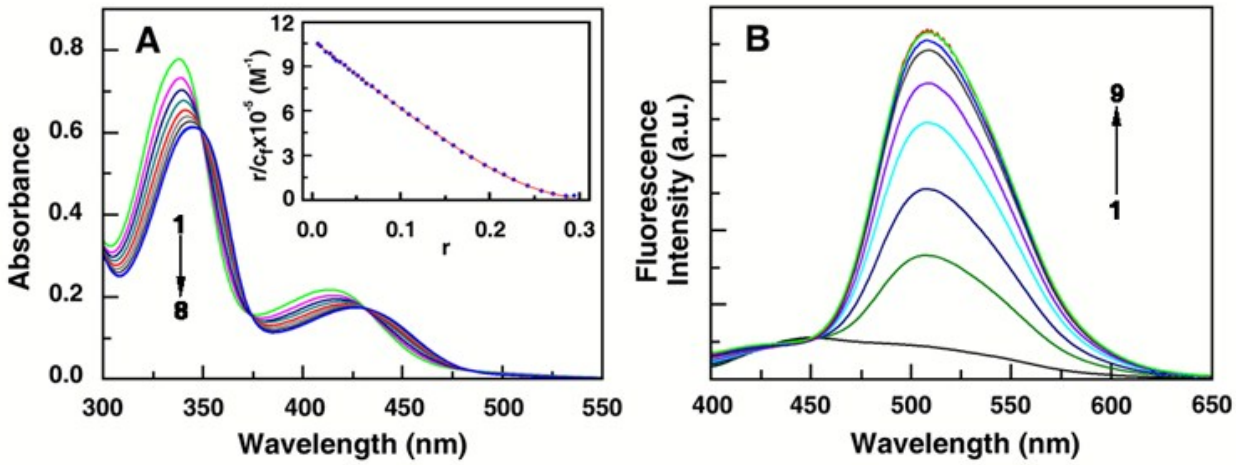

Fig. 1. Absorbance spectral changes in BER5 (35 µM, curve 1) **(**A) with increasing concentration of DNA upto 400 µM. Inset: Scatchard plot for the binding of BER5 to DNA obtained from McGhee-von Hippel analysis of spectrophotometric data. (B) Fluorescence spectra of BER5 (5 µM, curve1) with increasing concentration of DNA upto 70 µM of DNA.

RA-ART-08-2015-017214R1

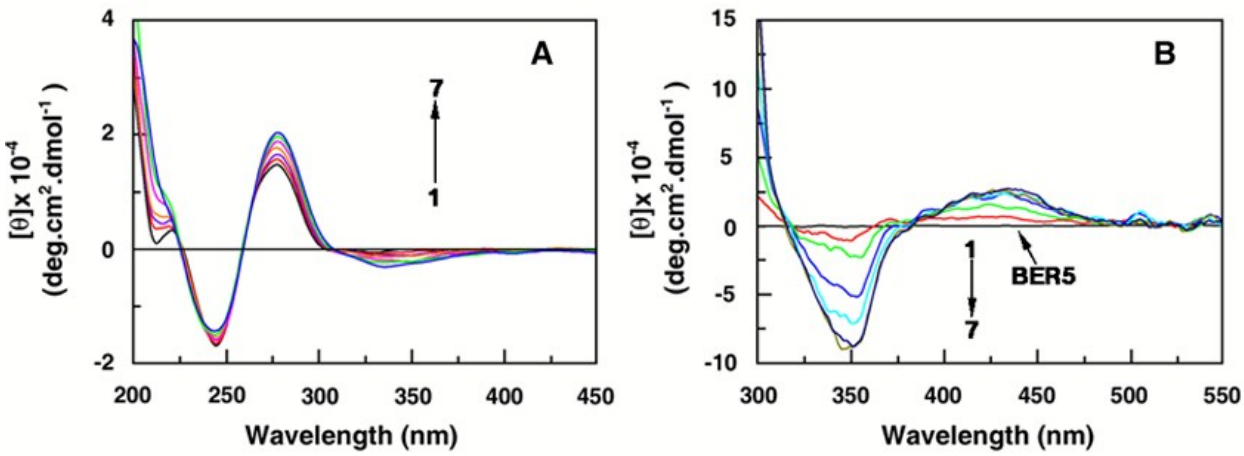

Fig. 2. Circular dichroism spectra (A) of DNA (30 µM, curve 1) with increasing concentration of BER5 upto 30 µM. Induced CD spectra (B) of BER5 (60 µM, curve 1) with increasing concentration of DNA upto 150 µM as represented by curves 2-7.

RA-ART-08-2015-017214R1

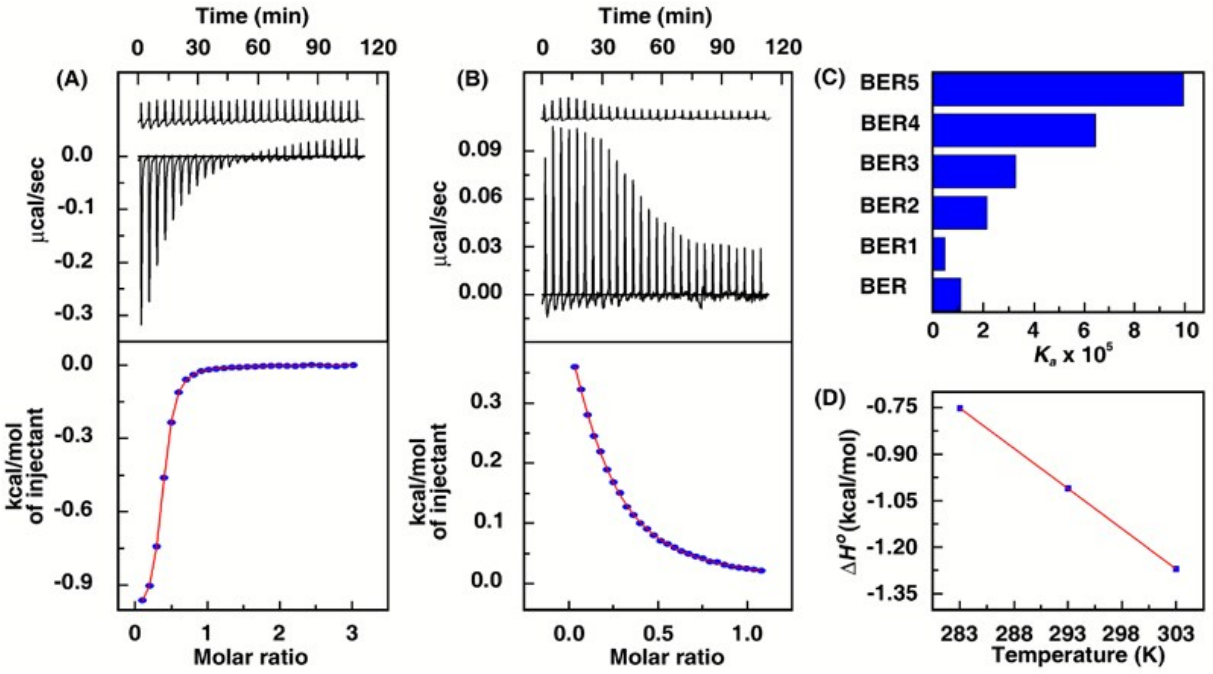

Fig. 3. ITC profiles of BER5 (A) and BER1 (B) (500µM) titrated into 50 µM and 100 µM, respectively, of DNA at 20 ^{o}C. The upper panels present the heat burst curves for the injection of samples and dilution profiles, and the bottom panels show the integrated heat data after correction of heat dilution. The symbols represent the data points that were fitted to a model 'one-site of binding sites' and the solid lines represent the best-fit data. (C) Variation of the binding constants of BER and its analogues-DNA from ITC studies. (D) Variation of standard molar enthalpy change with temperature for BER5-DNA interaction.

RA-ART-08-2015-017214R1

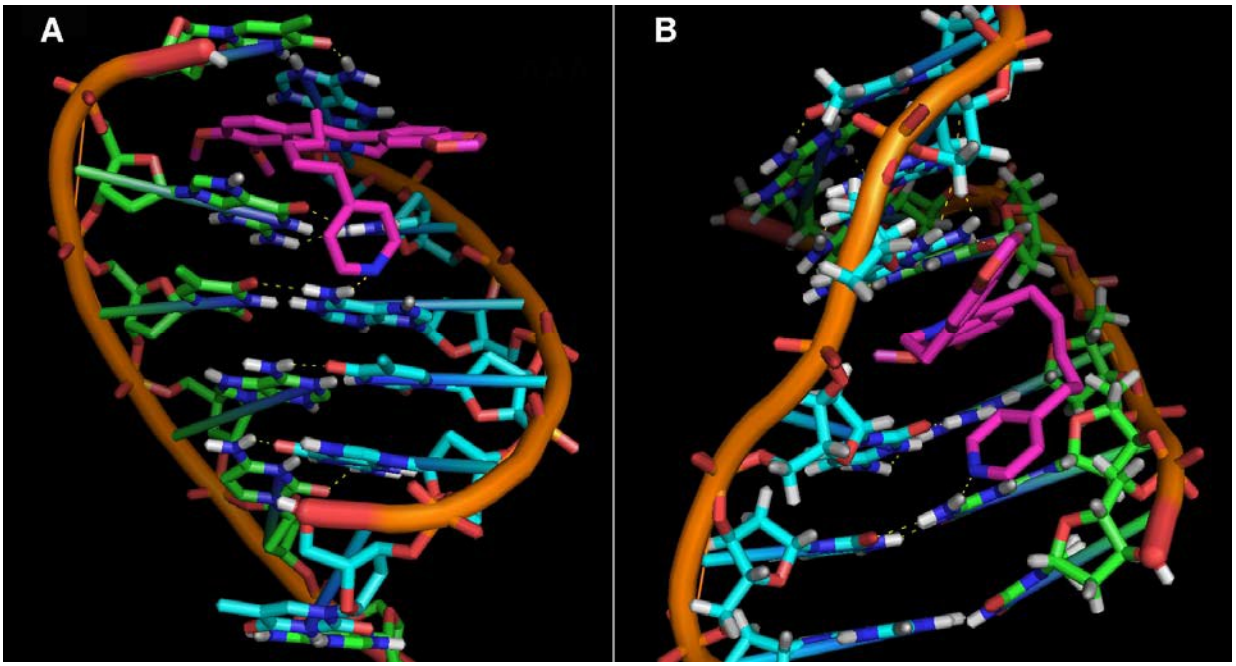

Fig. 4. Two docked conformation (A, B) of BER5 with two different DNA fragments.

RA-ART-08-2015-017214R1

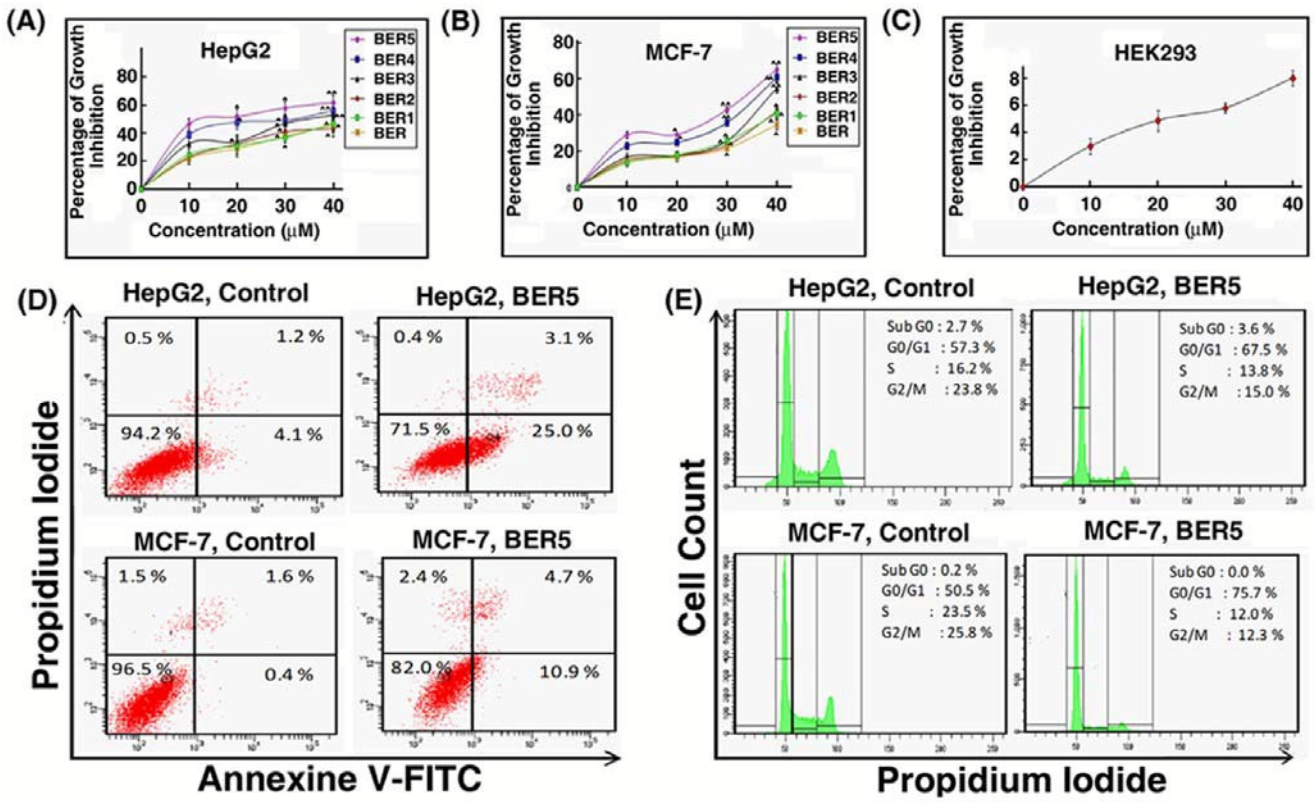

Fig. 5. Percentage growth inhibition of HepG2 (A) and MCF-7 (B) following treatment with BER, BER1, BER2, BER3, BER4 and BER5 (0, 10, 20,30 and 40 µM) for 24 h. (C) Growth inhibition of HEK293 cells following treatment with BER5 (0, 10, 20, 30 and 40 µM) for 24 h. (D) Flow cytometric analysis of apoptosis induction in HepG2 and MCf-7 cells after treatment with GI_{50} concentration of BER5 for 24 h.(E) Cell cycle analysis of BER5 (GI_{50}) treated HepG2 and MCF-7 cells for 24 h.

RA-ART-08-2015-017214R1

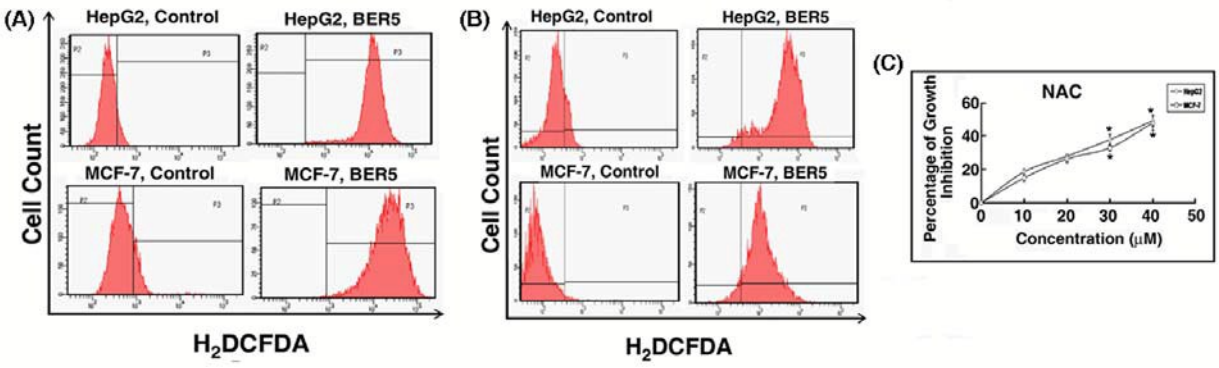

Fig. 6. Analysis of ROS generation in HepG2 (A) and MCF-7 (B)cells following treatment with BER5 along with NAC after 24 h by flow cytometry. (C) Percentage of growth inhibition in HepG2 and MCF-7 cells in presence of either NAC. Values are mean ± S.D and represent one of the three representative experiments. *P < 0.05.

RA-ART-08-2015-017214R1

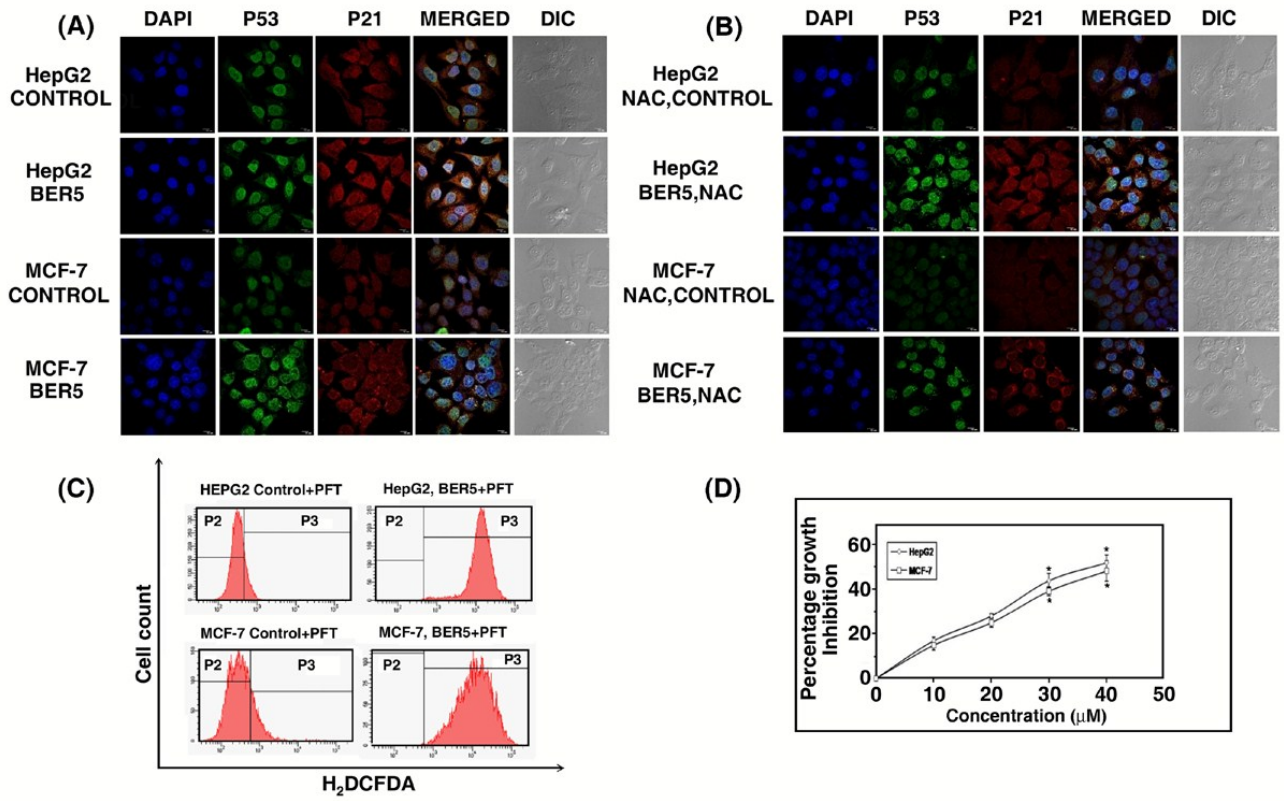

Fig. 7. (A) Up regulation of p53, p21 and subsequent nuclear translocation of p53 upon treatment of cells with BER5 (0 and GI_{50} concentration). Scale Bar=15 mm. Magnification at 40X.(B) Down regulation of p53 and p21 in the presence of NAC. Scale Bar=15 mm. Magnification at 40X. (C) ROS generation of HepG2 and MCF-7 cells after treatment with BER5 (GI_{50}) in the presence of PFT-α. (D) Percentage growth inhibition of HepG2 and MCF-7 cells in presence of pifthrin-α and BER5 with respect to the control (cells without treatment with BER5).

RA-ART-08-2015-017214R1

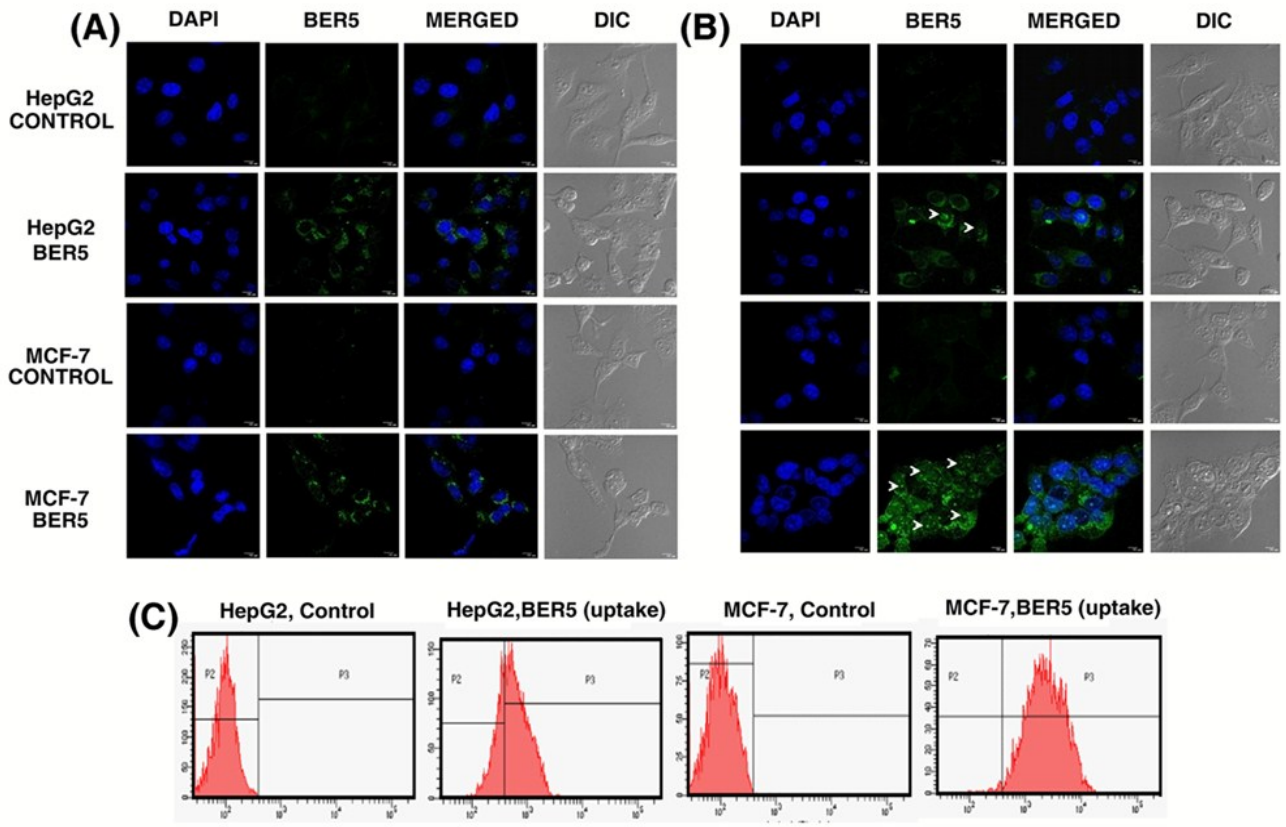

Fig. 8. Confocal microscopic images showed BER5 (GI_{50}) uptake at 12 h (A) and 24 h (B). (C) Flow cytometric analysis showed BER5 (GI_{50}) uptake after 24 h.

RA-ART-08-2015-017214R1

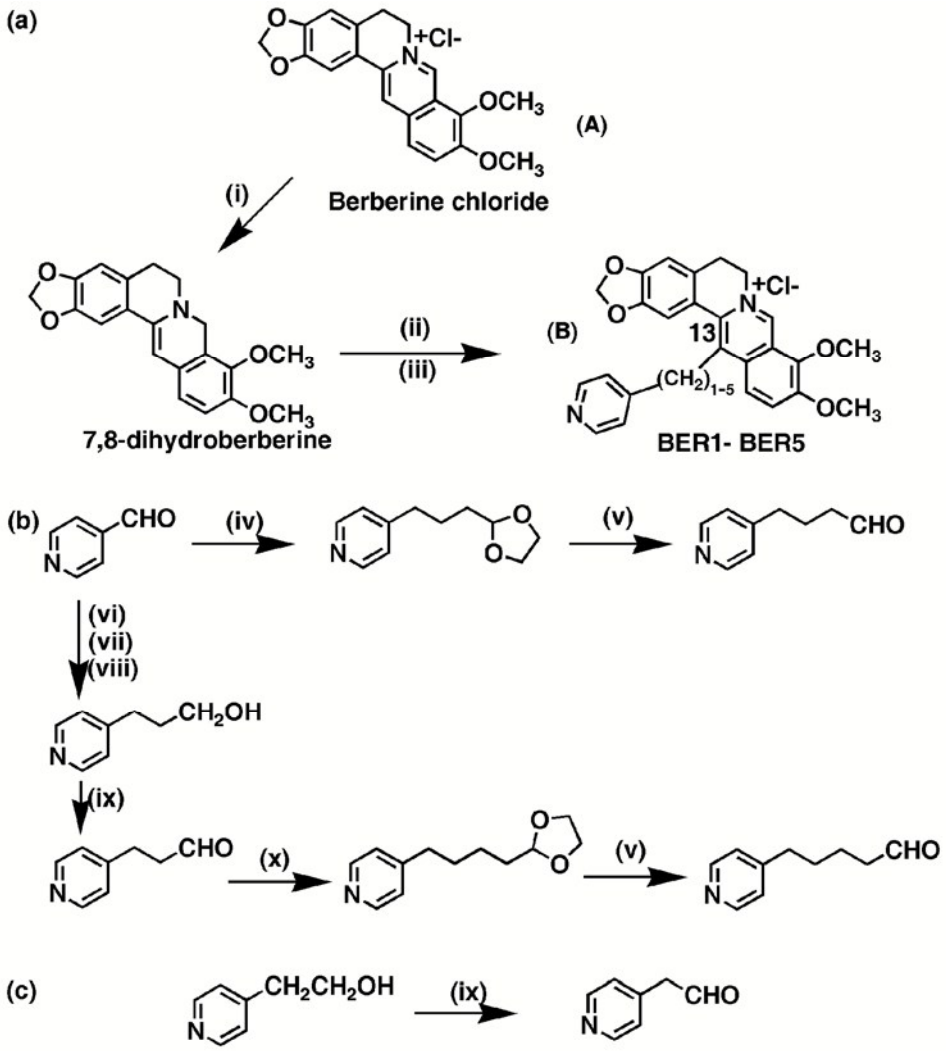

Scheme 1. (i) $NaBH_4$, pyridine, rt, 1h, (ii) $Py(CH_2)_{0\text{-}4}CHO$, 80% aq. EtOH, AcOH, 85°C, (iii) 2N HCl, rt, 2h. (iv) 2-(1,3-dioxolan-2-yl)ethyltriphenylphosphonium bromide, t-BuOK, THF, rt, (v) 60% aq TFA, rt, (vi) Ph_3P=CHCOOEt, 150°C, 2h, (vii) H_2, 10% Pd/C, EtOH, (viii) $LiAlH_4$, THS, rt, (ix) 1% TEMPO (2,2,6,6-tetramethyl-1-piperidinyloxy), NaClO, KBr, $NaHCO_3$, DCM, H_2O, (x) 2-(1,3-dioxolan-2 yl)methyltriphenylphosphonium bromide, t-BuOK, THF, rt, (ix).